ELSEVIER

Journal of Power Sources 93 (2001) 93–103

JOURNAL OF POWER SOURCES

www.elsevier.com/locate/jpowsour

Explicit analysis of impedance spectra related to thin films of spinel $LiMn_2O_4$

M. Mohamedi*, D. Takahashi, T. Uchiyama, T. Itoh, M. Nishizawa, I. Uchida

Department of Applied Chemistry, Graduate School of Engineering, Tohoku University, 07 Aramaki-Aoba, Aoba-Ku, Sendai 980-8579, Japan

Received 7 October 1999; received in revised form 17 May 2000; accepted 31 July 2000

Abstract

A uniform, dense film of spinel $LiMn_2O_4$ (0.1 μm thick) has been prepared by the electrostatic spray deposition (ESD) technique. The electroanalytical behavior of this electrode is elucidated by application of electrochemical impedance spectroscopy (EIS). The data have been modeled using an equivalent circuit approach. An excellent fit was found between measured data and an equivalent circuit, comprising Li^+ migration through surface film, potential-dependent charge transfer resistance, semiinfinite Warburg-type element, reflecting solid state Li^+ ion diffusion and a finite space Warburg-type element, describing both diffusion and accumulation of lithium at the very low frequency. The apparent chemical diffusion coefficient of lithium in the spinel phase was found within $10^{-12} < \tilde{D}_{Li} < 10^{-9}\,cm^2\,s^{-1}$ as a function of electrode potential with minima at the potentials corresponding to the voltammetric peaks. The intercalation capacitance was found $0.7 < C_L < 47\,mF\,cm^{-2}$ exhibiting maxima at the potentials corresponding to the voltammetric peaks.

Keywords: $LiMn_2O_4$; Electrostatic spray deposition; Thin film; Impedance; Modeling

1. Introduction

$LiMn_2O_4$ is an attractive cathode material for lithium secondary batteries [1–6]. Integration of such batteries into electronic devices at the chip level necessitates fabrication of thin film components of the battery. In order to comply with the requirements of the microelectronics fabrication technologies, the technique of preparing these films plays a major role. Various techniques, such as chemical vapor deposition and sputtering have been attempted to prepare thin films of diverse lithium battery components. Recently, Schoonman et al. [7–9] have utilized the electrostatic spray deposition (ESD) technique to fabricate thin films of lithium battery materials like $LiCoO_2$, $LiMn_2O_4$ and $LiNiO_2$. This technique offers several advantages, such as a simple and low-cost setup, low temperature synthesis and an easy control of the film composition and morphology.

Recently, we have successfully prepared dense films of spinel $LiMn_2O_4$ by ESD [10]. The electrochemical behavior of thus prepared films was investigated by means of cyclic voltammetry and potential step chronoamperometry in a solution of 1 M $LiClO_4$ in propylene carbonate (PC). It has been found that the oxidation and reduction of the film, which are accompanied by the extraction/insertion of lithium ions, occurred almost quantitatively around 4 V versus Li/Li^+ with excellent reversibility. The present paper aims at characterizing the performance of these electrodes by application of electrochemical impedance spectroscopy (EIS).

A major restriction of EIS characterization technique is that multiple equivalent circuits can be fitted to an impedance spectrum yielding somewhat equivocal results. Nonetheless, when the physicochemical situation of the electrochemical systems are clear and the choice of the model is based on parallel morphological spectroscopic, and electroanalytical studies, then it may considerably reduce the ambiguity and enable a selected circuit analog to be decided on. Another limitation concerns with the data analysis procedure itself. Complex linear least squares (CNLS) fitting of the data to a theoretical model and/or equivalent electrical circuit is the best method of quantitative analysis. Such fitting provides estimates of the parameters and their standard deviations [11–13]. Unfortunately, as noticed by Inzelt and Láng [14], in the majority of papers no standard deviations or relative standard deviation of the parameters are given. The goodness of fit is illustrated in the figure only. Control of the goodness of the fit is also

* Corresponding author. Fax: +81-22-214-8646.
E-mail address: mohamed@est.che.tohoku.ac.jp (M. Mohamedi).

0378-7753/01/$ – see front matter
PII: S0378-7753(00)00551-6

necessary, i.e. to check whether the derived parameters depend on the number of elements or not, or on the method of weighting.

2. Experimental details

$LiMn_2O_4$ cathodes were prepared by the electrostatic spray deposition (ESD). The ESD set-up used in this work was similar to that described in the literature [7–9]. Summarily, a high DC voltage (in a range of 0–20 kV) was applied between an electrically conductive substrate and a metal capillary nozzle, which is connected to a precursor solution. At an appropriate flow rate, the precursor solution was atomized at the orifice of the nozzle, generating the spray. The spray moves toward the heated substrate under electrostatic force, and owing to the pyrolysis of precursors, a thin layer is formed on the substrate surface. An ethanol precursor solution of 25 mM $LiNO_3$ + 50 mM $Mn(NO_3)_2$ was pumped at 0.1 ml/h to a stainless steel nozzle (0.8 mm i.d.), which was placed 2.5 cm above the gold flag substrate, heated typically at 400°C. The spraying nozzle was maintained at 12 kV against the electrode substrate. During the film deposition, the surface of the gold electrode was masked by means of an aluminum foil in order to limit the exposed area to a circle of 6 mm in diameter. The film thickness and morphology were studied by means of scanning electron microscope (JSM-5310LV), while the crystallographic structure was studied using a Cu Kα radiation with an incident angle of 2° (Shimadzu XD-D1).

The electrolyte was 1 M solution of $LiClO_4$ in a propylene carbonate (PC) (1 M = 1 mol/dm^3). The water content of the PC solution was less than 20 ppm. Electrochemical characterization of the cathode materiel was carried out using a three-electrode cell (T-cells). Lithium foils were used as the reference and counter electrodes.

EIS experiments were performed using Solartron's 1286 electrochemical interface and 1255-frequency response analyzer driven by the Corrware for Windows software (Scribner Associates). The impedance data generally covered the frequency range of 6 MHz to 10 kHz with an ac voltage signal of ±10 mV. The data were analyzed with a complex-nonlinear-least square program developed by Boukamp [15]. By means of this program, the optimized component values for a variety of different equivalent-circuit models could be rapidly evaluated. This procedure permits distinguishing between alternative models and an assessment of the physical interpretation of the components used in any given model.

In the following, Z_W, Z_{FLW} and Z_{FSW} are the semiinfinite Warburg, finite-length Warburg and finite-space Warburg diffusion impedance, respectively. The circuit description codes (CDC) of these elements are, *W*, *O* and *T*, respectively.

$$W = \frac{1}{Y_0(\sqrt{j\omega})} \tag{1}$$

$$O = \frac{\tanh(B\sqrt{j\omega})}{Y_0(\sqrt{j\omega})} \tag{2}$$

$$T = \frac{\coth(B\sqrt{j\omega})}{Y_0(\sqrt{j\omega})} \tag{3}$$

Y_0 and B are the fitted parameters. B depends on the diffusion coefficient, D_i, and the layer thickness, l, it follows that:

$$B = \frac{l}{\sqrt{D_i}} \tag{4}$$

The term Y_0 contains both the diffusion constant, the concentration, as well as the physical dimension of the system under study.

3. Results and discussion

Theoretical analysis of the complex impedance for charge injection involving layers of finite thickness was developed by Ho et al. [16] during the study of lithium injection and diffusion in thin solid-state WO_3 films. According to the authors, it is expected that the impedance of the electroactive films will exhibit at high frequency a charge transfer dominated regime. At lower frequencies, diffusion of charge in the film dominates the impedance results. The diffusion coefficient and the film thickness control the frequency range of the diffusion behavior. Finally, the finite thickness of the film will limit the extent of the diffusion behavior at low frequencies, and a ''redox capacitance'' is observed.

Fig. 1 presents a family of Nyquist diagrams and their corresponding Bode plots measured in the range of potentials from 3.80 to 4.40 V (at open circuit potential conditions) along with the anodic branch of the CV curve, i.e. during the course of deintercalation (due to scale limitation, the low frequency at the beginning (3.80 V) and the end (4.40 V) of the process is not displayed in the Nyquist plots). If the time constants for the different processes are sufficiently different, the diagram consists of:

1. A pronounced semicircle at the high-to-medium frequencies.
2. In the low frequency range (0.79–2 Hz), a straight line with a slope of 45° from the real axis is observed which corresponds to semiinfinite Warburg impedance.
3. At the very low frequencies, the 45° begins to give way to a more or less vertical line corresponding to finite space diffusion process or the differential intercalation capacity of the electrode at the measurement's potential [17,18].

3.1. Impedance analysis: methodology

Several equivalent circuits (EqCs) were sought which could describe the impedance response satisfactorily under all conditions examined. For the sake of comparison, we will

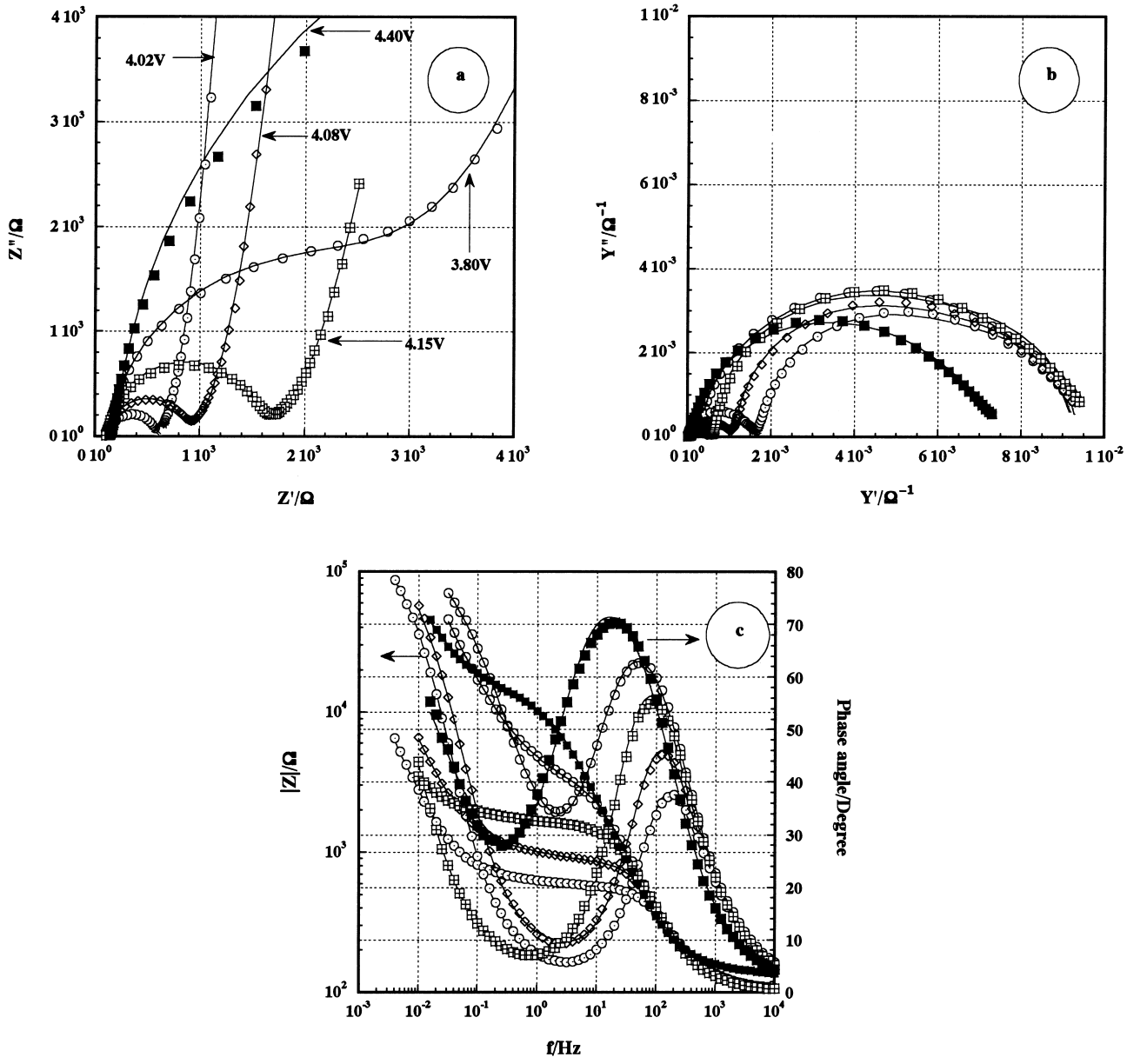

Fig. 1. A family of impedance plots of the $LiMn_2O_4$ (0.1 μm thick and 0.2 cm^2 area) electrode for various potentials during the course of deintercalation (the values of the potentials are indicated). Points represent experimental spectra and solid lines represent simulated curves according to Model IV of Fig. 2. (a) Nyquist plots; (b) admittance plots and (c) Bode representation.

restrict ourselves hereafter in presenting only circuits that are more consistent with the data and the physical-chemical properties of the system under study.

To study the differences between several possible models, there are rigorous ways to get an indication on how well the modeling function reproduces the actual data set. First, by observing the parameter values and their relative error estimate (%). The Chi-squared function (χ^2) also provides a good indication of the quality of the fit. Generally, the χ^2 statistic should be less than 10^{-6} if the data are said to fit within the noise level of the measurement. Therefore, a value of $10^{-5} \sim 10^{-4}$ indicates a reasonable good fit. χ^2 based on modulus weight factor [19] is defined here as follows:

$$\chi^2 = \sum_{i}^{N} \frac{(Z'_i - Z'_{i,sim})^2 + (Z''_i - Z''_{i,sim})^2}{Z'_i 2 + Z''_i 2} \quad (5)$$

where Z'_i and Z''_i are real and imaginary parts of experimental data, $Z'_{i,sim}$ and $Z''_{i,sim}$ are real and imaginary parts of simulated data.

Then, the actual data set can be observed in a graph of the relative residuals, $\Delta Z'_i$ and $\Delta Z''_i$ versus $\log \omega$. Following Boukamp [19] the residuals are defined by:

$$\Delta Z'_i = \frac{Z'_i - Z'_{i,sim}(\omega)}{|Z_{sim}(\omega)|} \quad \text{and} \quad \Delta Z''_i = \frac{Z''_i - Z''_{i,sim}(\omega)}{|Z_{sim}(\omega)|} \quad (6)$$

where $\omega = 2\pi f$ is the angular frequency of the ac-perturbation, $|Z_{sim}|$ is the vector length of the modeling function.

3.2. Expected models

In the absence of any surface layers, the impedance of an insertion electrode can be interpreted in terms of a simple network consisting of the bulk electrolyte resistance, R_e, in series with a $R\|C$ network made of two parallel current branches: (i) a faradaic-current branch represented by a charge transfer resistance, R_{ct}, serially connected to a Warburg impedance Z_W, and (ii) a nonfaradaic-branch consisting of the double layer capacitance, C_{dl}. This is the well-known Randles-circuit. An interface with a surface layer can be modeled by adding another $R_{sl}C_{sl}$ component (where "sl" stands for surface layer) to the original $R_{ct}C_{dl}$ network [11] (Fig. 2 Model I). Previously, Model I in Fig. 2 has been applied for example to lithium insertion in Sn-oxide film, in Ti-oxide film, in transparent Ti–Ce oxide films [20–22] and into $LiMn_2O_4$ and cobalt-doped $LiMn_2O_4$ [23]. In our work, the use of constant phase element (CPE) has been circumvented deliberately because our spectra were well modeled by ideal capacitors. Therefore, correlation to practical systems was preserved with practical physical significance. Model III in Fig. 2 is basically similar to the one applied by Aurbach et al. [24,25] to Li intercalation process into graphite and into transition metal oxides as Li_xCoO_2, Li_xNiO_2 and $Li_xMn_2O_4$ spinel electrodes. Z_{FLW} is a finite-length Warburg type element reflecting the Li solid-state diffusion. The C_{int} is a capacitor describing the accumulation of the intercalant (lithium) into the host materials. We have to emphasize that in Aurbach's model there are four serially connected R||C networks describing a multisurface layer. Their circuit is known as a combination of the Voigt-type analog and the generalized Frumkin and Melik Gaykazan (FMG) impedance. On the other hand, Model III in Fig. 2 applies for a one surface layer. We have modified Model I by incorporating a finite space Warburg-type element Z_{FSW} (Model IV in Fig. 2). The diffusion element, Z_{FSW}, describes the diffusion in a medium where the interface precludes the flow of the species and is represented by hyperbolic cotangent function [15,26,27].

3.3. Modeling results and interpretation

Table 1 provides a comparison of modeling quality of the different models proposed in Fig. 2 when applied to impedance spectra obtained at 4.02 V. It is plainly seen from the χ^2-values that Model I do not describe adequately the system. Models II–IV seem to refine to low χ^2-values with reasonable values for the physical processes represented. However, a visual inspection of the graphical output produced by the fitting program (Fig. 3) shows that only Models II and IV were capable of mimicking the spectra. It is also seen from Fig. 4 that error distributions versus frequency are the lowest (<2%) for Models II and IV.

We have also fitted our data to the complete Voigt-type analog and the generalized Frumkin and Melik Gaykazan (FMG) impedance used by Aurbach et al. [24,25]. The fitting results gave a good χ^2 of 2.10^{-5}. However, the error estimates for the $R\|C$ components were considerably high (10–20%). Moreover, we found no congruous variation of the circuits components with the applied potential. This might be due to the closeness of the time constants of the circuits, and/or some of the components have only a small contribution to the overall frequency dispersion.

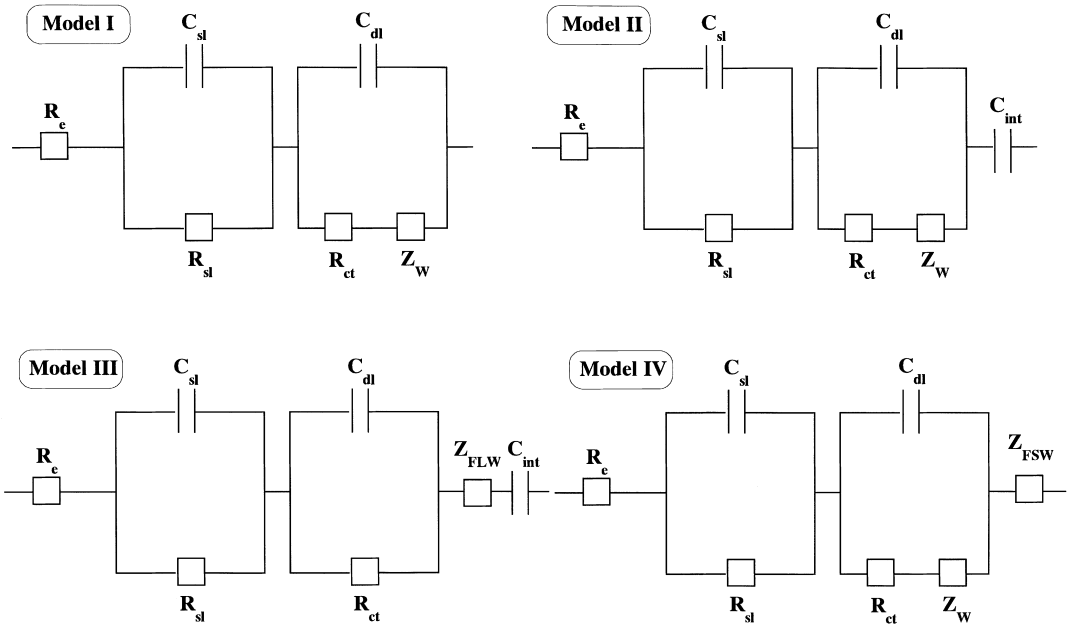

Fig. 2. Equivalent circuit representations of $LiMn_2O_4$ film electrode considered in this paper (see details in the text).

Table 1
Fitting parameters for models represented in Fig. 2 applied to impedance diagram recorded at 4.02 V[a]

	R_e/Ω	C_{dl}/mF	R_{ct}/Ω	C_{sl}/mF	R_{sl}/Ω	$Z_W Y_0 \times 10^{-3}$/ Ω^{-1} $s^{0.5}$	Z_{FLW} $Y_0 \times 10^{-3}$/ Ω^{-1} $s^{0.5}$	$B_{FLW}/s^{0.5}$	Z_{FSW} $Y_0 \times 10^{-3}$/ Ω^{-1} $s^{0.5}$	$B_{FSW}/s^{0.5}$	C_{int}/mF	χ^2
Model I	106 (10.8)	4.5 (18.5)	361 (8.09)	3.13 (136)	21.2 (85)	2.39 (8.1)	–	–	–	–	–	4.29×10^{-2}
Model II	108 (0.81)	4.9 (0.86)	426 (0.86)	4.44 (7.5)	35.1 (7.8)	5.63 (2.6)	–	–	–	–	7.7 (1.34)	4.32×10^{-4}
Model III	108 (1.18)	4.9 (3.31)	433 (1.29)	5.1 (10.9)	36.4 (12)	–	6.98 (4.26)	2.6 (6.28)	–	–	6.3 (1.49)	9.75×10^{-4}
Model IV	107 (0.61)	4.8 (1.45)	412 (0.66)	4.5 (6.35)	29.8 (5.8)	6.5 (3.05)	–	–	7.04 (6.3)	2.12 (5.8)	–	2.04×10^{-4}

[a] Numbers between brackets represent error estimates (%) for the individual components of the equivalent circuit. B_{FLW} and B_{FSW} are defined by Eq. (4) in the text.

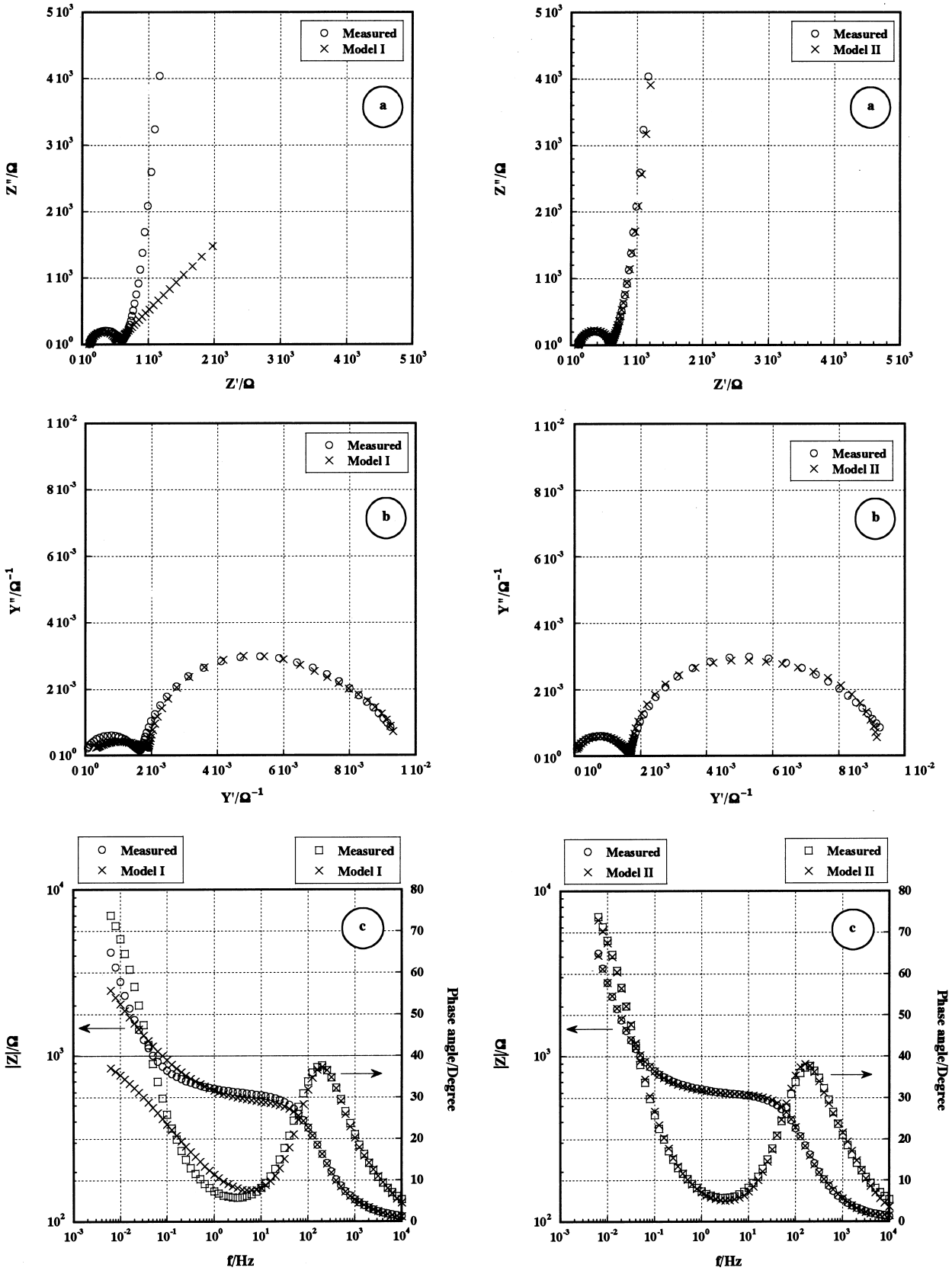

Fig. 3. Measured impedance spectra for the $LiMn_2O_4$ film electrode obtained at 4.02 V compared to spectra calculated following the models shown in Fig. 2. (a) Nyquist plots; (b) admittance plots and (c) Bode representation.

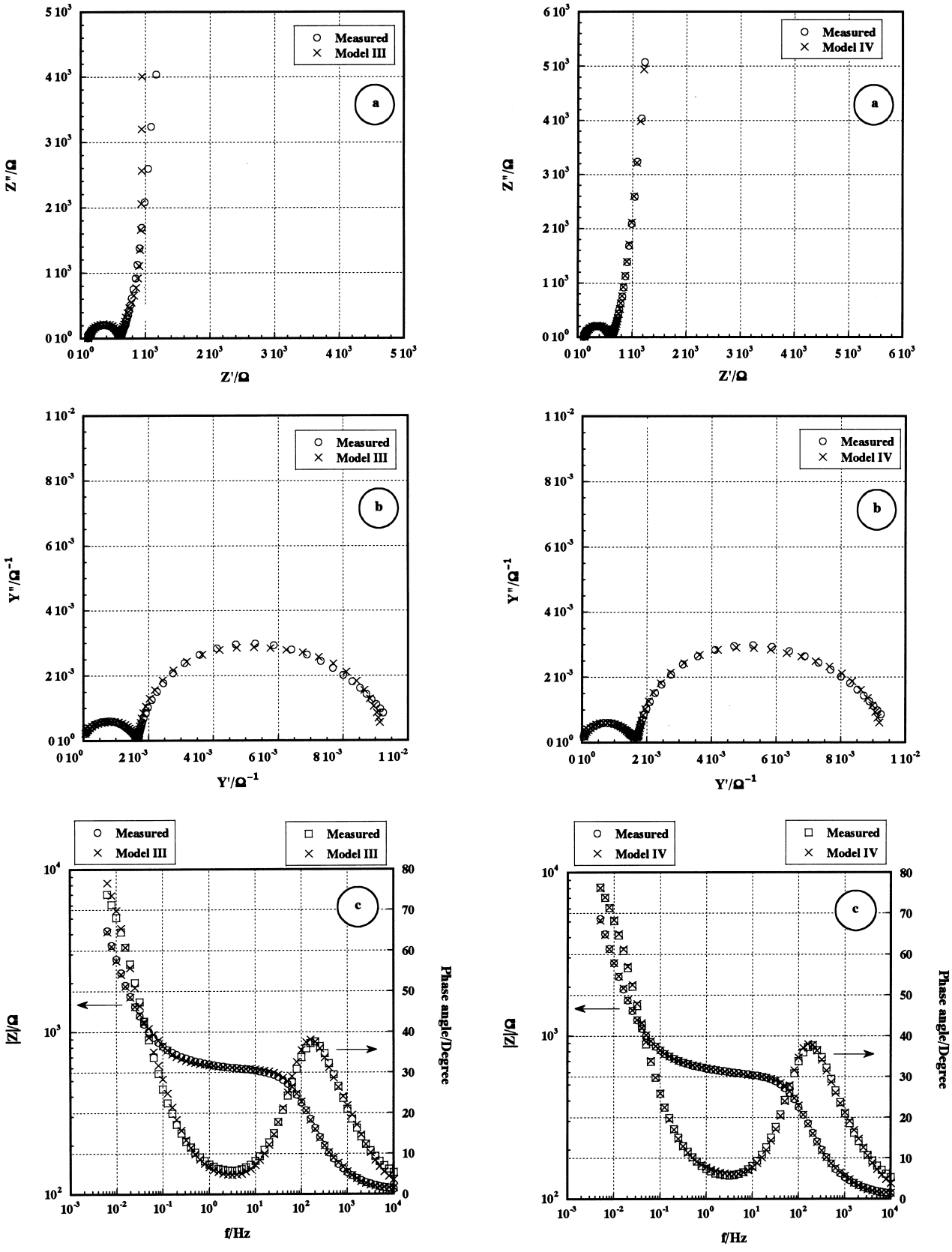

Fig. 3. (*Continued*).

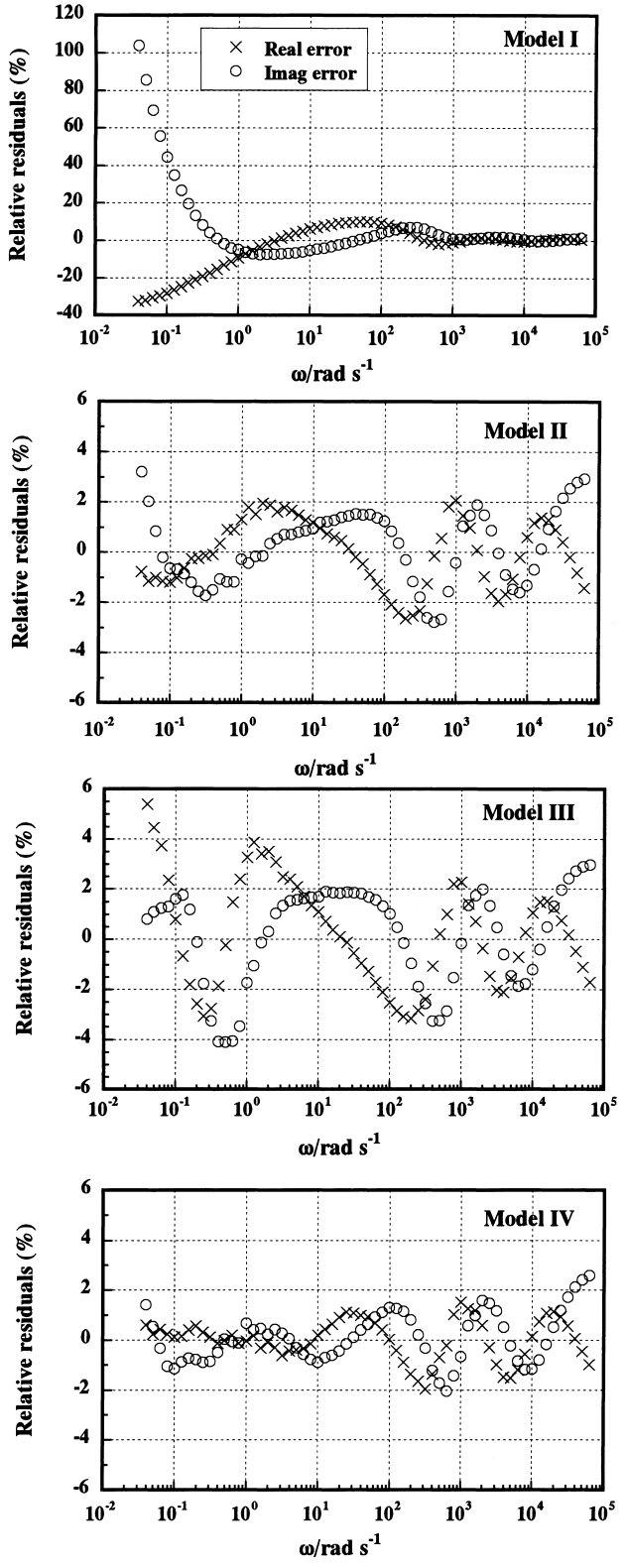

Fig. 4. Relative residual plots for the fits presented in Fig. 3. Real error and imaginary error were calculated according to Eq. (6).

A tentative interpretation of Model IV can be made by comparison with Goodenough et al. [11] analysis. According to the authors, two different physical processes may be involved to account for the addition of an $R\|C$ to the Randles equivalent circuit: (i) adsorption of Li^+ or propylene carbonate onto the surface of the electrode without charge transfer and (ii) formation of an ionically conducting but electronically insulating surface layer at the electrode surface. To distinguish between these two models Goodenough et al. [11] have studied the time dependence of the ac-impedance response and the variation of the circuit parameters with applied voltage. Their results have shown that only the surface layer model contains equivalent circuit parameters that vary in a self-consistent manner with the electrochemical processes they represents as the cell conditions are varied.

Conclusively, in agreement with Goodenough et al. [11], we ascribe the $R_{sl}C_{sl}$ to the resistance for Li^+ ion migration through the surface film and film capacitance, as probably formed by electrolyte decomposition product. It is not trivial then to assign the second $R\|C$ to the electron transfer resistance of the intercalation reaction and capacitance of a double layer. Although Model II describes adequately the observed response, the fitting results were further evaluated for all applied potentials according to Model IV using Z_{FSW} instead of C_{int} because of the straightforward physical significance of the former parameter. Results of fitting are exhibited in Fig. 1.

3.4. Model parameters

We observe that R_{ct} is high for high potentials (3.8 and 4.4 V) (Fig. 5). The charge transfer resistance being high for high potentials is consistent with the observations on the voltammograms where the current is zero (see Fig. 6, here-

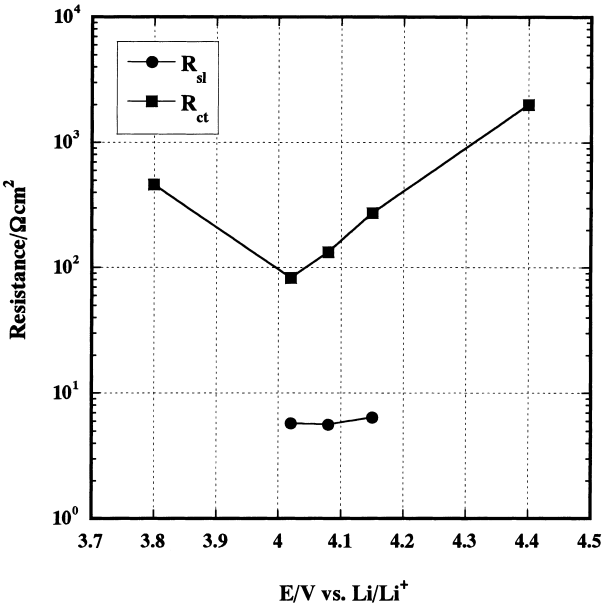

Fig. 5. Plots of the charge transfer resistance, R_{ct}, and the surface layer resistance, R_{sl} vs. potential. R_{ct} and R_{sl} were obtained by fitting the experimental impedance spectra with Model IV of Fig. 2.

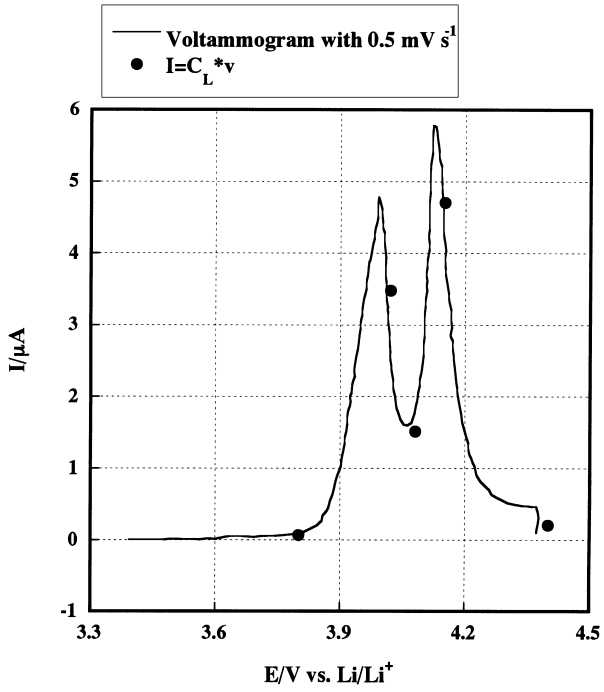

Fig. 6. Comparison of the voltammetric response of a $LiMn_2O_4$ electrode at 0.5 mV/s (solid line) with $C_L \times v$ (points). C_L is the film redox capacitance obtained from Eq. (14) and v is the scan rate used in obtaining the actual voltammogram.

after). The surface layer resistance, R_{sl} was found more or less constant in the 4.02–4.15 V potential range (Fig. 5). The values of R_{sl} at 4.40 and 3.80 V have been left since the error estimates obtained in the fitting on the R_{sl} and C_{sl} parameters were extremely large.

The values of the surface-layer capacitance were in the range of 23–32 mF cm^{-2} (Fig. 7), in agreement with those reported by for the pure spinel [23]. The C_{dl} values ranging from 23–34 mF cm^{-2} (Fig. 7) are characteristics of double layer capacitance and support the equivalent circuit interpretation.

3.5. Determination of the exchange current density

The charge transfer resistance is related to the exchange current density, i_0, by the equation:

$$R_{ct} = \frac{RT}{nFi_0} \tag{7}$$

The exchange current densities were calculated using Eq. (7) for various applied potentials. The results are shown in Fig. 8. The exchanged current density lies between 0.01 and 0.4 mA/cm^2. We found that i_0 exhibits a maximum at the potential of the first CV peak and then monotonously decreases for higher potentials.

3.6. Determination of Li-ion chemical diffusion coefficient

The chemical diffusion coefficient $\tilde{D}_{Li}$ may be obtained by either several ways:

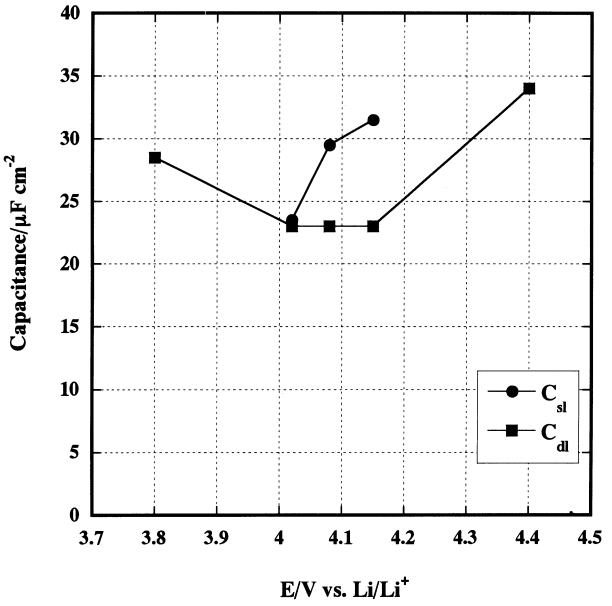

Fig. 7. Plots of the double layer capacitance, C_{dl}, and the surface layer capacitance, C_{sl} vs. potential. C_{dl} and C_{sl} were obtained by fitting the experimental impedance spectra with Model IV of Fig. 2.

- Under semiinfinite conditions$(\omega \succ\succ 2\tilde{D}_{Li}/l^2)$ in the case when the time constants of the different physical processes occurring at the electrode are separated, $\tilde{D}_{Li}$ can be obtained from an analysis of the Warburg impedance, Z_W [16], which is expressed in the complex plane as:

$$Z_W = \frac{V_m}{\sqrt{2}nFA\tilde{D}_{Li}^{1/2}}\frac{dE}{dx}(1-j)\omega^{-1/2} = \sigma(1-j)\omega^{-1/2} \tag{8}$$

where σ is the Warburg coefficient, V_m the molar volume of the host structure, dE/dx the slope of the coulometric titra-

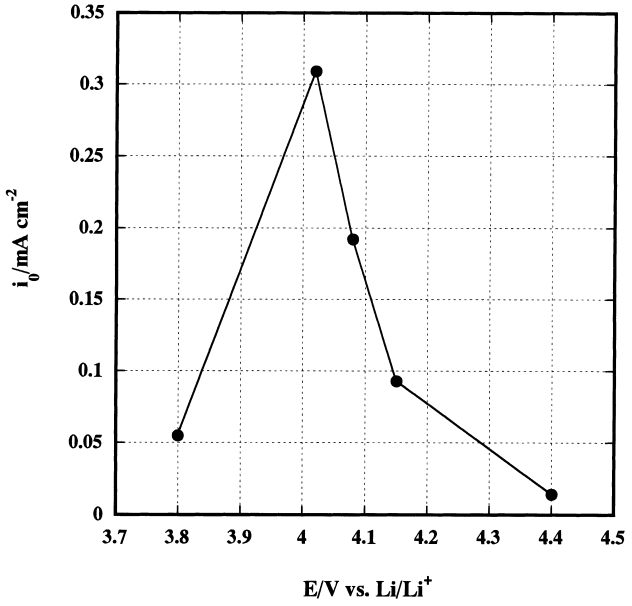

Fig. 8. Exchange current density, i_0 vs. potential; i_0 was determined by means of Eq. (7).

tion curve versus mobile ion concentration x at each x value, l the maximum length of the diffusion pathway, and n the number of equivalent ($n = 1$). The Warburg coefficient can be obtained from the slope of the Z'' versus $\omega^{-1/2}$ or Z' versus $\omega^{-1/2}$.

In the general case, the Warburg impedance in the faradaic branch must be related to the diffusion coefficients of the insertion ion in both the electrolyte and the electrode. In our experimental spectra, the observed semiinfinite Warburg impedance might be confounded with diffusion-controlled process in solution and in the oxide. In order to remove all doubts about the meaning of the Warburg behavior, we have studied the influence of electrolyte concentration, especially in the low frequency range related to lithium diffusion in the oxide. No significant variation in the Warburg slope with the electrolyte concentration was observed in the range of 1 M to 10 mM $LiClO_4$. This indicates that, for our experimental conditions (1 M $LiClO_4$), lithium diffusion in the bathing electrolyte is not a limiting factor, and proves that the semiinfinite Warburg behavior observed in our experimental spectra is relevant to lithium diffusion in the solid phase.

- If the homogeneous diffusion ($\omega \succ\succ 2\tilde{D}_{\mathrm{Li}}/l^2$) is observed (last part of the diagram), the current is approximately 90° out of phase with voltage. Under this condition, the real part of the impedance is independent of the frequency. The extrapolated real intercept of the straight-line region gives rise to the limiting low frequency resistance, R_{L}, defined by Ho et al. [16]:

$$Z' = R_{\mathrm{L}} = \frac{V_{\mathrm{m}}}{nFA}\frac{\mathrm{d}E}{\mathrm{d}x}\frac{l}{3\tilde{D}_{\mathrm{Li}}} \tag{9}$$

The authors also express the imaginary part of the impedance as:

$$Z'' = \frac{1}{\omega C_{\mathrm{L}}} = \frac{V_{\mathrm{m}}}{nFA}\frac{\mathrm{d}E}{\mathrm{d}x}\frac{1}{\omega l} \tag{10}$$

$$\frac{1}{C_{\mathrm{L}}} = \frac{\mathrm{d}Z''}{\mathrm{d}\omega^{-1}} \tag{11}$$

Thus, in the range of the impedance phase angle approaches $\pi/2$, the value of the redox capacitance, C_{L} can be determined graphically from the slope of Eq. (11). Therefore, $\tilde{D}_{\mathrm{Li}}$ may be deduced from Eqs. (9) and (11)

$$\tilde{D}_{\mathrm{Li}} = \frac{l^2}{3R_{\mathrm{L}}C_{\mathrm{L}}} \tag{12}$$

- From the so-called finite space diffusion Warburg impedance [15,16,26–28] as this element reflects both diffusion and accumulation (capacitive behavior at the very low frequencies):

$$Z_{\mathrm{FSW}} = \left(\frac{\tau}{C_{\mathrm{L}}}\right)\left(\frac{j\omega l^2}{\tilde{D}_{\mathrm{Li}}}\right)^{-1/2}\coth\left(\frac{j\omega l^2}{\tilde{D}_{\mathrm{Li}}}\right)^{-1/2} \tag{13}$$

where $\tau = l^2/\tilde{D}_{\mathrm{Li}}$ is the diffusion constant.

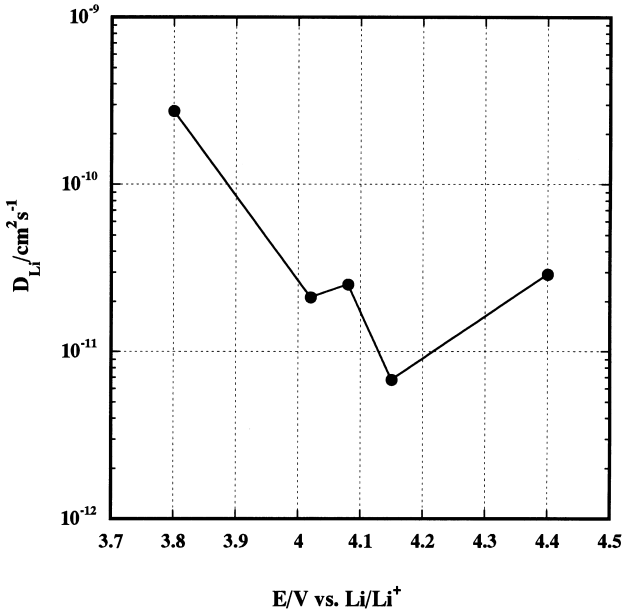

Fig. 9. Semi-logarithmic representation of the variation of the chemical diffusion coefficient of Li-ions vs. potential for the $LiMn_2O_4$ electrode.

The determination of R_{L} is not precise and an inaccuracy is introduced in the calculation of the diffusion coefficient using Eq. (12). More accurate values of the $\tilde{D}_{\mathrm{Li}}$ can be deduced from either the semiinfinite diffusion (Eq. (8)) or the finite space diffusion domain using Eq. (13).

Since the Warburg-type impedance was assessed as being film diffusion process where the diffusion layer thickness, l, can replace the thickness of film (0.1 mm) through which the diffusion takes place. Therefore, the ratio $l/\sqrt{\tilde{D}_{\mathrm{Li}}}$ in Eq. (13) was determined from the fitted parameter B (Eq. (4)). Fig. 9 shows that $10^{-12} < \tilde{D}_{\mathrm{Li}} < 10^{-9}$ during deintercalation process. As also demonstrated in this figure, log $\tilde{D}_{\mathrm{Li}}$ versus E exhibits two distinct minima at the anodic CV peak potentials.

3.7. Determination of the intercalation capacitance, C_L

The low frequency capacitance, was estimated using:

$$Y_0 = \frac{\sqrt{\tilde{D}_{\mathrm{Li}}}C_{\mathrm{L}}}{l\tau} \tag{14}$$

Direct comparison of the intercalation capacitance, C_{L} determined from EIS data with the voltammetric response can be made by multiplying C_{L} by the scan rate, v employed in the voltammetric experiments. In theory, these data are exactly equivalent to that obtained from CV response of an ideal film electrode at sufficiently slow scan rates (conditions where thin layer electrochemical behavior is observed) [29], or that the film be sufficiently thin to insure that the effects of diffusional charge transport in the film phase is absent. In our previous study [10], we found that that current peak was strictly proportional to scan rate only at $v \leq 0.5$ mV/s. Fig. 6 demonstrates good agreement of *I–E*

curve reconstructed from C_L data with the corresponding cyclic voltammogram obtained at a 0.5 mV/s scan rate.

4. Conclusions

Characterization of $LiMn_2O_4$ thin film made by ESD technique has been achieved by means of impedance spectroscopy. Experimental spectra have been modeled following rigorous criteria. The derived model contains a $R\|C$ network related to surface layer via which Li^+ migrates, a Randles-circuit describing the electron transfer and the lithium ions solid state diffusion and a finite space diffusion element describing both lithium diffusion and accumulation. Specific parameters of interest determined in this investigation of $LiMn_2O_4$ thin films were: (i) diffusion coefficient, (ii) redox capacitance, (iii) surface film capacitance, resistance, and (iv) exchange-current density. An effective method of testing robustness of the model will be to change the experimental conditions (electrolyte, temperature, film thickness, etc.) to observe how well the model predicts the changes, i.e. in order to find physically reasonable dependencies that help to discriminate adequately between the derived parameters. This will be the topic of our next paper.

Acknowledgements

This work was supported by grant-in-aid for Scientific Research (B) (No. 0555297) and (A) (No. 10555297) and Priority Area (No. 10131211, 11118213) for ''Electrochemistry of Ordered Interfaces'' from the Ministry of Education, Science, Sports and Culture of Japan.

References

[1] B. Scrosati, in: J. Lipkowski, P.N. Ross, (Eds.), Electrochemistry of Novel Materials, VCH Publishers, New York, 1994 (Chapter 3).
[2] P.G. Bruce, Chem. Commun. (1997) 1817.
[3] T. Ohzuku, M. Kitagawa, T. Hirai, J. Electrochem. Soc. 137 (1990) 769.
[4] A.H. Gemeay, H. Nishiyama, S. Kuwabata, H. Yoneyama, J. Electrochem. Soc. 142 (1995) 4190.
[5] D. Guyomard, J.M. Tarascon, J. Electrochem. Soc. 139 (1992) 937.
[6] K. Kanamura, H. Naito, T. Yao, Z. Takehara, J. Mater. Chem. 6 (1996) 33.
[7] C. Chen, E.M. Kelder, J. Schoonman, J. Electrochem. Soc. 144 (1997) L289.
[8] C. Chen, E.M. Kelder, M.J.G. Jak, J. Schoonman, Solid State Ionics 86/87 (1996) 1301.
[9] C. Chen, E.M. Kelder, P.J.J. van der Put, J. Schoonman, J. Mater. Chem. 6 (1996) 765.
[10] M. Nishizawa, T. Uchiyama, K. Dokko, K. Yamada, T. Matsue, I. Uchida, Bull. Chem. Soc. Jpn. 71 (1998) 2011.
[11] M.G.S.R. Thomas, P.G. Bruce, J.B. Goodenough, J. Electrochem. Soc. 132 (1985) 1521.
[12] J.R. MacDonald, D.R. Franceschetti, J. Electroanal. Chem. 307 (1991) 1.
[13] B.A. Boukamp, Solid State Ionics 20 (1986) 31.
[14] G. Inzelt, G. Láng, J. Electroanal. Chem. 378 (1994) 34.
[15] B.A. Boukamp, Equivalent Circuit Users Manual, University of Twente, 1989.
[16] C. Ho, I.D. Raistrick, R.A. Huggins, J. Electrochem. Soc. 127 (1980) 343.
[17] M.D. Levi, D. Aurbach, J. Phys. Chem. B101 (1997) 4630.
[18] M.D. Levi, D. Aurbach, J. Phys. Chem. B101 (1997) 4641.
[19] B. A Boukamp, J. Electrochem. Soc. 142 (1995) 1885.
[20] G.A. Niklasson, C.G. Granqvist, Phys. Rev. B54 (1996) 2968.
[21] M. Strømme, J. Isidorsson, G.A. Niklasson, C.G. Granqvist, J. Appl. Phys. 80 (1996) 233.
[22] M. Strømme, A. Azens, G.A. Niklasson, C.G. Granqvist, J. Appl. Phys. 81 (1997) 6432.
[23] P. Arora, B.N. Popov, R.E. White, J. Electrochem. Soc. 145 (1998) 807.
[24] D. Aurbach, M.D. Levi, E. Levi, G. Salitra, B. Markovsky, H. Teller, J. Electrochem. Soc. 145 (1998) 3024.
[25] M.D. Levi, G. Salitra, B. Markovsky, H. Teller, D. Aurbach, U. Heider, L. Heider, J. Electrochem. Soc. 146 (1999) 1279.
[26] S.R. Taylor, E. Gileadi, Corros. Sci. 51 (1995) 664.
[27] J. Ross MacDonald, Impedance Spectroscopy, Emphasizing Solid Materials and Applications, Wiley, New York, 1987, p. 88.
[28] I. Rubinstein, J. Risphon, S. Gottesfeld, J. Electrochem. Soc. 133 (1986) 729.
[29] A.J. Bard, L.R. Faulkner, Electrochemical Methods-Fundamentals and Applications, Wiley, New York, 1980.